Substituted 4,4′-Stilbenoid NCN-Pincer Platinum(II) Complexes. Luminescence and Tuning of the Electronic and NLO Properties and the Application in an OLED

Guido D. Batema,[†] Martin Lutz,[‡] Anthony L. Spek,[‡,#] Cornelis A. van Walree,[†] Celso de Mello Donegá,[§] Andries Meijerink,[§] Remco W. A. Havenith,[⊥] Javier Pérez-Moreno,[¶] Koen Clays,[¶] Michael Büchel,[□] Addy van Dijken,[□] David L. Bryce,[■] Gerard P. M. van Klink,[†,○] and Gerard van Koten*[,†]

Organic Chemistry and Catalysis, Faculty of Science, Utrecht University, Padualaan 8, 3584 CH Utrecht, The Netherlands, Crystal and Structural Chemistry, Faculty of Science, Utrecht University, Padualaan 8, 3584 CH Utrecht, The Netherlands, Condensed Matter and Interfaces, Faculty of Science, Utrecht University, Princetonplein 1, 3508 TA Utrecht, The Netherlands, Theoretical Chemistry Group, Faculty of Science, Utrecht University, Padualaan 8, 3584 CH Utrecht, The Netherlands, Molecular and Nanomaterials, University of Leuven, Celestijnenlaan 200D, 3001 Leuven, Belgium, Philips Research Laboratories Eindhoven, High Tech Campus 4 (WAG11), 5656 AE Eindhoven, The Netherlands, and Department of Chemistry and Centre for Catalysis Research and Innovation, University of Ottawa, Ottawa, Ontario, K1N 6N5, Canada

Received April 11, 2007

A series of 4,4′-disubstituted organic−organometallic stilbenes, i.e., the 4′-substituted stilbenoid-NCN-pincer platinum(II) complexes [PtCl(NCN-R-4)] (NCN-R-4 = $[C_6H_2(CH_2NMe_2)_2$-2,6-R-4$]^-$ in which R = $C_2H_2C_6H_4$-R′-4′ with R′ = NPh_2, NMe_2, OMe, $SiMe_3$ H, I, CN, NO_2) (**1**−**8**), were studied for their electronic, electrochemical, and NLO properties. Complex **7** was also chemically oxidized using $Cu(II)Cl_2$, yielding the $[Pt(IV)Cl_3(NCN(C_2H_2C_6H_4$-CN-4′)-4)] complex **11**. In contrast to **1** and **7**, **11** did not show luminescent properties in solution at room temperature. In the solid state (X-ray crystallography) **11** has an overall bent structure, with the pincer moiety and the cyano group beneath the plane of the central double bond. Stilbenoid pincer complex **1** (R′ = NPh_2) was also studied with UV/vis spectroscopy in a series of different solvents. The compound shows an intense low-energy transition band, appearing at a lower energy (λ_{max} = 374–379 nm) than **2** (R′ = NMe_2), which contains a stronger donor group. The UV/vis absorption data of a selected series of stilbenoid pincer platinum complexes were interpreted in terms of a qualitative orbital model based on DFT and TD-DFT calculations. The trends observed in the transition energies correlate well with the donor/acceptor properties of the substituents. It was shown that the HOMO–LUMO gap of the stilbenoid pincer platinum compounds decreases when going from an electron-neutral group (R′ = H) toward an electron-donating (R′ = NMe_2) or -accepting (R′ = NO_2) group. The fluorescence properties of **1** were also investigated using fluorescence and laser spectroscopy, showing that the metal center favors nonradiative decay from the excited state to the ground state. For **7** (R′ = CN), solid-state ^{13}C CP/MAS NMR measurements were performed, and a value of $^1J(^{13}C,^{195}Pt) = 1003 \pm 15$ Hz was obtained for the C_{ipso} carbon, reflecting π-contributions in the carbon−metal bond. The cyclic voltammetry study on the complexes revealed an irreversible oxidation from Pt(II) to Pt(IV). In general the oxidation potential is influenced by the electronic character of the R′ substituent. The influence of the *para* R′ substituent on the hyperpolarizability of the compound was investigated using the femtosecond (frequency-resolved) HRS technique. For **1**−**7** good β_{zzz} values were measured (β_{zzz} ranging from (164–1324) × 10^{-30} esu) with the highest value for **6** (R′ = I). The higher β_{zzz} values were found for the compounds that contain a low-energy UV/vis absorption band and/or a large absorption coefficient. Donor–acceptor complexes **7** and **8** were successfully applied in an organic light-emitting diode (OLED). In the electroluminescence spectrum of **7** (R′ = CN) a low-energy emission band was observed at 643 nm. This band also appeared in the solid-state luminescence spectra of **7**, however, only at low temperatures (298–15 K). The emission band was assigned to result from a triplet excited state. The present study shows that the introduction of a NCN-pincer platinum fragment in a donor–acceptor stilbenoid molecule leads to complexes that have promising NLO properties. These compounds can now successfully be applied in OLED devices, although the performances of the devices have to be improved to become interesting for practical applications.

Introduction

Much interest exists in the synthesis and study of conjugated organic materials. Recently also the incorporation of organometallic fragments in conjugated functional materials has been explored.[1] The introduction of an organometallic fragment offers possibilities for modification and tuning of the electronic, physical, and/or optical properties of these materials. Connection of the metal as an electron donor or acceptor group to another donor or acceptor group, either directly or via a conjugated π-network, leads to intense and low-energy intramolecular charge transfer (ICT) transitions.[2] By changing the ligands, the metal itself, or the oxidation state of the metal complex, the transition energy of such a push–pull system can be influenced

* To whom correspondence should be addressed. E-mail: g.vankoten@uu.nl.
[†] Organic Chemistry and Catalysis, Faculty of Science, Utrecht University.
[‡] Crystal and Structural Chemistry, Utrecht University.
[#] Author to whom crystallographic inquiries may be directed: E-mail: a.l.spek@chem.uu.nl
[§] Condensed Matter and Interfaces, Utrecht University.
[⊥] Theoretical Chemistry Group, Utrecht University.
[¶] University of Leuven.
[□] Philips Research Laboratories Eindhoven.
[■] University of Ottawa.
[○] Present address: DelftChemTech, Faculty of Applied Sciences, Delft University of Technology, Julianalaan 136, 2628 BL Delft, The Netherlands.

(1) Wolf, M. O. *J. Inorg. Organomet. Polym. Mater.* **2006**, *16*, 189–199.
(2) Cariati, E.; Pizzotti, M.; Roberto, D.; Tessore, F.; Ugo, R. *Coord. Chem. Rev.* **2006**, *250*, 1210–1233.

10.1021/om700352z CCC: $40.75
Publication on Web 03/25/2008

Chart 1

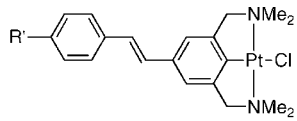

R' = NPh_2 (**1**), NMe_2 (**2**), OMe (**3**), $SiMe_3$ (**4**), H (**5**), I (**6**), CN (**7**), NO_2 (**8**)

in order to obtain a high hyperpolarizability.[3] Therefore the attractive nonlinear optical (NLO)[4] and organic light-emitting diode (OLED)[5] properties of organometallic and coordination complexes are widely studied.

Recently we developed a series of novel 4,4′-disubstituted organic−organometallic stilbenes (Chart 1), i.e., the 4′-substituted stilbenoid-NCN-pincer platinum(II) complexes [Pt-Cl(NCN-R-4)] (NCN-R-4 = $[C_6H_2(CH_2NMe_2)_2$-2,6-R-4$]^-$ in which R = $C_2H_2C_6H_4$-R′-4′ with R′ = NMe_2, OMe, $SiMe_3$ H, I, CN, NO_2) (**2**−**8**).[6] In these stilbenoid compounds the PtCl grouping is present as one of the *para* substituents and in π-electronic terms is acting as a donor substituent. The acceptor group is located at the other *para* position in the stilbenoid system. The platinum metal is fixed in the tridentate coordinating NCN pincer ligand to the effect that the aryl plane and the Pt coordination plane are (almost) coplanar. By changing the substituent R′ while keeping the pincer platinum fragment constant it was possible to modulate the electronic properties of the complex. Linear correlations were found between the ^{13}C and ^{195}Pt NMR chemical shift of the C_{ipso} carbon atom and the Pt nucleus, respectively, and the Hammett substituent parameter σ_p of the *para* substituent. The photophysical properties of three of the compounds, i.e., those with R′ = NMe_2 (**2**), CN (**7**), and NO_2 (**8**), were studied and showed fluorescent properties. The above-mentioned series was extended with the new stilbenoid pincer platinum complex **1**, with R′ = NPh_2. The diphenylamine donor group extends the π-framework resulting from hetero-atomic π-conjugation[7] of the coplanar diphenylamine fragment with the stilbenoid platinum system. As N-phenyl substitution can lead to improved material properties in nonlinear optics and for hole transport layers in electroluminescent devices,[8,9] the potential application of the stilbenoid pincer metal complexes as functional materials is substantially extended.

In the present study the change of the electrochemical and NLO properties of **1**−**8** in solution, induced by the different *para* substituents, has been investigated using cyclic voltammetry. The first hyperpolarizability tensor component β_{zzz} was determined using the hyper-Rayleigh scattering (HRS) technique. TD-DFT calculations were performed on a selected series of stilbenoid pincer platinum compounds in order to interpret the UV/vis spectra of these molecules.

From previous studies it is known that NCN-pincer platinum(II) complexes can be chemically oxidized in solution, forming a stable NCN-Pt(IV) complex.[10–13] Therefore luminescent Pt(II) complex **7** was chemically oxidized, and the resulting Pt(IV) complex was studied for its physical, electronic, and solid-state properties. In order to determine the one-bond $^1J(^{13}C, ^{195}Pt)$ coupling constant, which is not easy to obtain from the solution spectra, the nature of the Pt−C_{ipso} interaction in **7** was studied using solid-state ^{13}C CP/MAS NMR measurements. For the fluorescent donor–acceptor stilbenoid pincer complexes **7** and **8** the application in an organic light-emitting diode (OLED) was studied. The electroluminescence spectrum of this OLED revealed a new low-energy excitation band, and therefore **7** was further investigated in a solid-state luminescence study.

Results and Discussion

Synthesis and Characterization. The synthesis of the 4′-NPh_2-substituted stilbenoid pincer platinum complex started with the synthesis of diethyl diphenylaminobenzylphosphonate ester **9**[14,15] and [PtCl(NCN-CHO-4)] **10**.[6] Horner−Wadsworth−Emmons conditions were used to couple **9** with **10** (Scheme 1), affording [PtCl(NCN($C_2H_2C_6H_4$−NPh_2-4′)-4)] (**1**) as the pure *trans* isomer in good yield (93%).

The chemical oxidation of the stilbenoid NCN Pt(II) system [Pt(II)Cl(NCN($C_2H_2C_6H_4$-CN-4′)-4)] (**7**) was achieved by using $Cu(II)Cl_2 \cdot 2H_2O$ (2.1 equiv) as the oxidant (Scheme 2), following a previous study from our group.[10,16] The oxidation reaction was carried out in a mixture of CH_2Cl_2 and MeOH, from which the coproduct Cu(I)Cl precipitated. The resulting product [Pt(IV)Cl_3(NCN($C_2H_2C_6H_4$-CN-4′)-4)] (**11**) was isolated in 69% yield. Upon oxidation, the square-planar Pt(II) arrangement converts into an octahedral one (Pt(IV)).

Stilbenoid pincer platinum complexes **1** and **11** were fully characterized using ^1H, $^{13}C\{^1H\}$, and $^{195}Pt\{^1H\}$ NMR and IR spectroscopy, elemental analysis, and mass spectrometry. Complex **11** was also analyzed by single-crystal X-ray structure determination, showing the octahedral Pt(IV) arrangement, as mentioned above.

Crystal Structure of 11. Crystals of **11** suitable for single-crystal X-ray structure determination were obtained by slow evaporation of a dichloromethane solution. The compound crystallizes with two independent molecules in the asymmetric unit (Figure 1). The two molecules have very similar bond lengths and angles (Table 1) but differ in the conformation of the 4-cyanostyryl fragment (Figure 2). The overall shape of both molecules is bent, i.e., the distances of the C_{ipso} carbon atoms

(3) Calabrese, J. C.; Cheng, L. T.; Green, J. C.; Marder, S. R.; Tam, W. *J. Am. Chem. Soc.* **1991**, *113*, 7227–7232.

(4) (a) Le Bozec, H.; Renouard, T. *Eur. J. Inorg. Chem.* **2000**, 229–239. (b) Lacroix, P. G. *Eur. J. Inorg. Chem.* **2000**, 339–348. (c) Di Bella, S. *Chem. Soc. Rev.* **2001**, *30*, 355–366. (d) Coe, B. J. In *Comprehensive Coordination Chemistry II*; McCleverty, J. A. , Meyer, T. J. , Eds.; Elsevier Pergamon: Oxford, U.K., 2004; Vol. 9, pp 621–687. (e) Powell, C. E.; Humphrey, M. G. *Coord. Chem. Rev.* **2004**, *248*, 725–756. (f) Coe, B. J. *Acc. Chem. Res.* **2006**, *39*, 383–393.

(5) (a) Slinker, J.; Bernards, D.; Houston, P. L.; Abruña, H. D.; Bernhard, S.; Malliaras, G. G. *Chem. Commun.* **2003**, 2392–2399. (b) Richter, M. M. *Chem. Rev.* **2004**, *104*, 3003–3036. (c) Holder, E.; Langeveld, B. M. W.; Schubert, U. S. *Adv. Mater.* **2005**, *17*, 1109–1121. (d) Ma, B.; Djurovich, P. I.; Garon, S.; Alleyne, B.; Thompson, M. E. *Adv. Funct. Mater.* **2006**, *16*, 2438–2446. (e) Evans, R. C.; Douglas, P.; Winscom, C. J. *Coord. Chem. Rev.* **2006**, *250*, 2093–2126.

(6) Batema, G. D.; van de Westelaken, K. T. L.; Guerra, J.; Lutz, M.; Spek, A. L.; van Walree, C. A.; de Mello Donegá, C.; Meijerink, A.; van Klink, G. P. M.; van Koten, G. *Eur. J. Inorg. Chem.* **2007**, 1422–1435.

(7) Sato, K.; Yano, M.; Furuichi, M.; Shiomi, D.; Takui, T.; Abe, K.; Itoh, K.; Higuchi, A.; Katsuma, K.; Shirota, Y. *J. Am. Chem. Soc.* **1997**, *119*, 6607–6613.

(8) Kuntz, J. F.; Schneider, R.; Walcarius, A.; Fort, Y. *Tetrahedron Lett.* **2005**, *46*, 8793–8797.

(9) He, Q. G.; Lin, H. Z.; Weng, Y. F.; Zhang, B.; Wang, Z. M.; Lei, G. T.; Wang, L. D.; Qiu, Y.; Bai, F. L. *Adv. Funct. Mater.* **2006**, *16*, 1343–1348.

(10) Terheijden, J.; van Koten, G.; de Booys, J. L.; Ubbels, H. J. C.; Stam, C. H. *Organometallics* **1983**, *2*, 1882–1883.

(11) van Beek, J. A. M.; van Koten, G.; Wehman-Ooyevaar, I. C. M.; Smeets, W. J. J.; van der Sluis, P.; Spek, A. L. *J. Chem. Soc., Dalton Trans.* **1991**, 883–893.

(12) van Koten, G. *Pure Appl. Chem.* **1990**, *62*, 1155–1159.

(13) van Koten, G.; Terheijden, J.; van Beek, J. A. M.; Wehman-Ooyevaar, I. C. M.; Muller, F.; Stam, C. H. *Organometallics* **1990**, *9*, 903–912.

(14) Plater, M. J.; Jackson, T. *Tetrahedron* **2003**, *59*, 4673–4685.

(15) Zheng, S. J.; Barlow, S.; Parker, T. C.; Marder, S. R. *Tetrahedron Lett.* **2003**, *44*, 7989–7992.

(16) Albrecht, M.; van Koten, G. *Angew. Chem., Int. Ed. Engl.* **2001**, *40*, 3750–3781.

Scheme 1. Synthesis of 1[a]

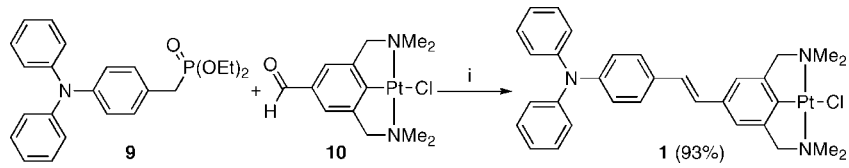

[a] Reagents and conditions: (i) a. *t*-BuOK, THF, 2 h; b. H_2O.

Scheme 2. Oxidation of 7 toward 11[a]

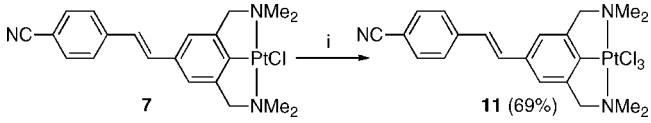

[a] Reagents and conditions: (i) $CuCl_2 \cdot 2H_2O$ (2.1 equiv), CH_2Cl_2:MeOH (1:1), 24 h, rt.

C1 from the least-squares plane of the central double bond (C*n*4−C*n*13−C*n*14−C*n*15 with $n = 1$, 2) are 0.620(5) and 0.442(5) Å. For the corresponding *para* carbon atoms C*n*18 the distances are 0.244(6) and 0.349(6) Å, respectively.

In both molecules the least-squares plane of the pincer fragment and the benzonitrile ring are mutually nonplanar, with torsion angles between the two planes of 38.4(3)° (residue 1) and 60.3(3)° (residue 2).

Comparison of the molecular structure of **11** with the earlier reported [$PtCl_3$(NCN)] complex[10,13] shows a similar distorted octahedral geometry around the platinum center, containing two axial chloride atoms. The distortion of the octahedral geometry is reflected in the N−Pt−N angle of 162.35(18)–162.39(19)° and the small N−Pt−C_{ipso} angles of 80.8(2)–81.6(2)°. The carbon atoms of the benzylic substituents (C7 and C10) are positioned above and below the plane defined by C1−N1−Pt1−N2−Cl1. For the two puckered five-membered metallacycles, torsion angles with magnitudes of 32.4(6)–36.1(6)° were found for the Pt1−N1−C7−C2 and Pt1−N2−C10−C6 bonds. The platinum to C_{ipso} (Pt−C) distances are in the range 1.952(6)–1.957(5) Å, as expected.[10,13] Furthermore there is a significant difference between the Pt−Cl bond lengths of the two axial chloride atoms (2.3148(16)–2.3396(17) Å) and the meridonial chloride atom (2.4421(16)–2.4598(16) Å), reflecting the *trans* influence[17] of C_{ipso} of the NCN fragment on the *trans*-Pt−Cl bond, weakening this interaction. A comparison between the molecular structure of **7** (Pt(II)), which was reported earlier,[6] and **11** (Pt(IV)) in the solid state reveals longer bonding distances of the Pt−C, Pt−N, and the Pt−Cl bonds in **11**, reflecting the formal +4 oxidation state of the platinum center.

NMR and IR Spectroscopy. Selected ^{13}C and ^{195}Pt NMR and IR data are listed in Table 2, along with data for **7**.[6] For **1** the obtained NMR data are in agreement with the NMR data from the previous study on related stilbenoid pincer platinum complexes **2**−**8**.[6] Noteworthy is that a single doublet belonging to one of the vinylic protons was observed at $\delta = 6.92$ ppm, with coupling constant $^3J(H,H) = 16$ Hz, confirming that also in solution **1** has a *trans* configuration. The other vinylic proton signal was part of a complex pattern at 7.07–7.01 ppm, together with signals from aromatic protons.

In the $^{13}C\{^1H\}$ NMR spectrum of **1** the ^{13}C NMR resonances of the C_{ipso} (to platinum) carbon appeared at 146.6 ppm. The $^{195}Pt\{^1H\}$ NMR spectrum of **1** showed a signal for the platinum center at –3163 ppm. This fits into the trend that was found when the ^{195}Pt chemical shift of *para*-substituted [PtCl(NCN($C_2H_2C_6H_4$-R′-4′)-4)] complexes was plotted versus the Hammett substituent parameter (σ_p) of the respective R′ substituent.[6] This observed correlation points to a long distance electronic interaction between the R′ substituent and the platinum center. Compound **1**, with $\delta = -3163$ ppm and σ_p $NPh_2 = -0.22$,[18] is positioned in the correlation between the donating OMe and NMe_2 groupings, confirming the donating character of the diphenylamino group. Recently, Marder and co-workers assessed the electron-transfer-donor strengths and π-donor strengths of various amines using density functional theory calculations.[19]

For the stilbenoid NCN-pincer Pt(IV)Cl_3 complex **11** the (CH_3)$_2$N and the ArCH_2N protons are found at 3.06 and 4.42 ppm, respectively, with proton−platinum coupling constants of $^3J(H,Pt) \approx 29$ and 30 Hz, respectively. The ArCH_2N protons of **11** are shifted about 0.37 ppm to lower field compared to starting Pt(II)Cl complex **7**.[6] Related to this, the three-bond platinum coupling constants $^3J(H,Pt)$ of the CH_2 and CH_3 protons of the CH_2NMe_2 groups in **11** ($^3J(H,Pt) = 29$–30 Hz) are smaller compared to those found in **7** ($^3J(H,Pt) = 38$–46 Hz), reflecting a decreased interaction of the metal center with these protons. These observations are similar to those for related Pt(II) → Pt(IV) oxidation reactions in which [PtX(NCN)] (X = Cl or Br) complexes are converted to the corresponding [Pt(IV)X_3(NCN)] complexes.[10,20] The same shifts are observed in the $^{13}C\{^1H\}$ NMR spectrum of **11**. The largest effect is observed for C_{ipso}, which shifts from 148.6 (in **7**) to 144.9 ppm (in **11**), reflecting an increase of negative charge at this atom as a result of further Pt−C bond polarization. The $^{13}C\{^1H\}$ NMR (δ *C*N) and IR spectroscopic data of the nitrile groups in **7** and **11** (Table 2) seem not to be sensitive to the different oxidation states of the *para*-$PtCl_n$ ($n = 1$ or 3) grouping. The ^{13}C chemical shifts for both **7** and **11** are 119 ppm, while the intensive νCN stretch vibrations are located at 2223 (**7**) and 2222 (**11**) cm^{-1}, respectively.

Solid-State NMR Measurements. In order to get more information about the nature of the C_{ipso}−platinum bond, the ^{13}C RAMP-CP/MAS NMR spectroscopic data, δ $^{13}C_{ipso}$, and $^1J(^{13}C, ^{195}Pt)$ of solid **7** were measured. In particular the aromatic region was studied in more detail, because the C_{ipso} carbon of **7** is found at 152 ppm. Data acquired at 11.75 T revealed what appeared to be one of the two ^{195}Pt satellites of the C_{ipso} with the other satellite buried beneath one of the other aromatic carbon resonances (see Figures 3a and 3b).

To confirm this interpretation, a spectrum was acquired at 21.1 T, which increased the resolution. At this ultrahigh magnetic field strength the two ^{195}Pt satellites are clearly resolved, as shown in Figure 3c. The splitting corresponds to $^1J(^{13}C,^{195}Pt) = 1003 \pm 15$ Hz. The one-bond coupling constant is in almost exact agreement with the value found for the solution spectrum of the parent pincer platinum complex

(17) Coe, B. J.; Glenwright, S. J. *Coord. Chem. Rev.* **2000**, *203*, 5–80.

(18) Hansch, C.; Leo, A.; Taft, R. W. *Chem. Rev.* **1991**, *91*, 165–195.

(19) Kwon, O.; Barlow, S.; Odom, S. A.; Beverina, L.; Thompson, N. J.; Zojer, E.; Bredas, J.-L. ; Marder, S. R. *J. Phys. Chem. A.* **2005**, *109*, 9346–9352.

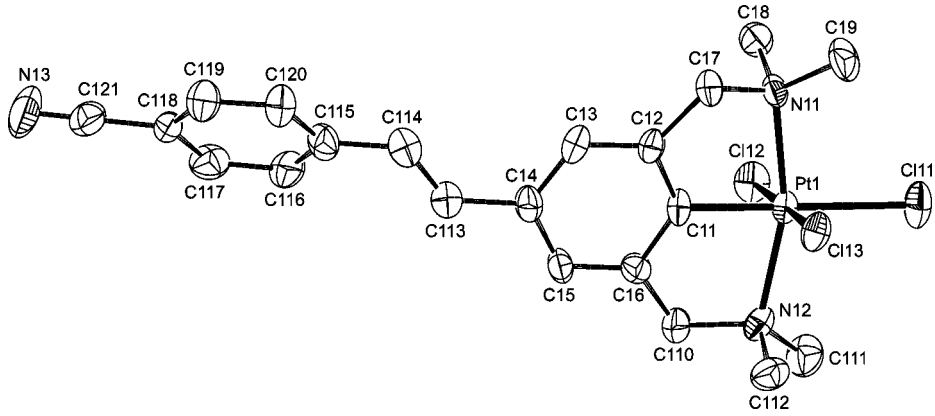

Figure 1. Displacement ellipsoid plot (50% probability level) of **11** in the crystal. Only one of two independent molecules is shown. Hydrogen atoms are omitted for clarity.

Table 1. Selected Bond Lengths [Å], Angles [deg], and Torsion Angles [deg] of [$PtCl_3$(NCN($C_2H_2C_6H_4$CN-4′)-4)] (11)

residue 1		residue 2	
Pt1−C11	1.957(5)	Pt2−C21	1.952(6)
Pt1−N11	2.150(5)	Pt2−N21	2.140(5)
Pt1−N12	2.161(5)	Pt2−N22	2.136(5)
Pt1−Cl11	2.4598(16)	Pt2−Cl21	2.4421(16)
Pt1−Cl12	2.3300(16)	Pt2−Cl22	2.3396(17)
Pt1−Cl13	2.3148(16)	Pt2−Cl23	2.3160(16)
C113−C114	1.300(10)	C213−C214	1.315(9)
C121−N13	1.126(10)	C221−N23	1.140(9)
N11−Pt−N12	162.35(18)	N21−Pt2−N22	162.39(19)
C11−Pt1−N11	81.5(2)	C21−Pt2−N21	81.6(2)
C11−Pt1−N12	80.9(2)	C21−Pt2−N22	80.8(2)
C11−Pt1−Cl11	179.07(19)	C21−Pt2−Cl21	178.25(17)
C11−Pt1−Cl12	90.14(17)	C21−Pt2−Cl22	89.40(17)
C11−Pt1−Cl13	89.02(17)	C21−Pt2−Cl23	90.33(17)
Pt1−N11−C17−C12	−32.4(6)	Pt2−N21−C27-C22	−35.3(6)
Pt1−N12−C110−C16	−36.1(6)	Pt2−N22−C210-C26	−34.4(6)
C14−C113−C114−C115	169.6(7)	C24−C213−C214-C215	−172.4(6)
		angle between planes	
[C11−C12−C13−C14−C15-C16], [C115−C116−C117−C118−C119−C120]	38.4(3)	[C21−C22−C23−C24−C25-C26], [C215−C216−C217−C218−C219−C220]	60.3(3)

Table 2. NMR[a] and IR[b] Data of 1, 7, and 11

[$PtCl_n$(NCN($C_2H_2C_6H_4$-R′-4′)-4)]	δ $^{13}C_{ipso}$ (ppm)	δ ^{195}Pt (ppm)[c]	IR νC≡N (cm^{-1})
1 (R′ = NPh_2), $n = 1$	146.6	−3163	
7 (R′ = CN), $n = 1$[d]	148.6	−3138	2223
11 (R′ = CN), $n = 3$	144.9	−1504	2222

[a] Solution in CD_2Cl_2. [b] ATR spectra. [c] Na_2PtCl_6 (1.0 M in D_2O) was used as external reference ($\delta = 0$ ppm). [d] Data obtained from ref 5.

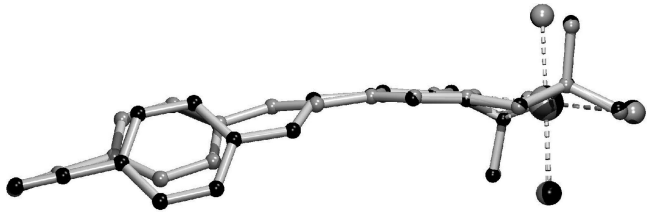

Figure 2. Quaternion fit based on the pincer moieties of the two independent molecules in the crystal structure of **11**. Molecule 1 is drawn in gray, molecule 2 in black.

[PtCl(NCN)] ($^1J(^{13}C,^{195}Pt)$, $CDCl_3 = 1002$ Hz).[21] The magnitude of the coupling constant, as well as δ $^{13}C_{ipso} = 152.0$ ppm, were used to simulate the observed coupling pattern (Figures 3b and 3c). The spectra also show excellent resolution of crystallographically nonequivalent carbons in the region at 60–50 ppm (Figure 3a), e.g., four methyl resonances are resolved.

The value of $^1J(^{13}C,^{195}Pt) = 1003 \pm 15$ Hz may be compared to previously reported one-bond platinum−carbon coupling constants.[22,23] Values of $^1J(^{13}C,\ ^{195}Pt)$ for σ-bonded methyl carbons are quite small (e.g., 475 ± 2 Hz for *trans*-[$CH_3Pt(AsMe_3)_2$-(MeNC)][PF_6]).[24,25] Values of $^1J(^{13}C,^{195}Pt)$ for σ-bonded aromatic carbons tend to fall in the range 600–900 Hz, with $^1J(^{195}Pt,^{13}C) = 502 \pm 1$ Hz representing a particularly small value (for *trans*-[$(C_6H_5)Pt(AsMe_3)_2(L)$][PF_6] where L is the cyclic carbene :$CCH_2CH_2CH_2O$)[26] and 1186 Hz, representing a particularly large value, for [Pt(cod)(2-C_4H_3S)(2-C_4H_3S)].[27] Another large $^1J(^{13}C,\ ^{195}Pt)$ value of 1175 Hz was reported for

(20) Lagunas, M. C.; Gossage, R. A.; Spek, A. L.; van Koten, G. *Organometallics* **1998**, *17*, 731–741.
(21) Terheijden, J.; van Koten, G.; Muller, F.; Grove, D. M.; Vrieze, K.; Nielsen, E.; Stam, C. H. *J. Organomet. Chem.* **1986**, *315*, 401–417.
(22) Mann, B. E.; Taylor, B. F. *13C NMR Data for Organometallic Compounds*; Academic Press: London, 1981.
(23) Pregosin, P. S. *Transition Metal Nuclear Magnetic Resonance*; Elsevier: Amsterdam, 1991.
(24) Chisholm, M. H.; Clark, H. C.; Manzer, L. E.; Stothers, J. B.; Ward, J. E. H. *J. Am. Chem. Soc.* **1973**, *95*, 8574–8583.
(25) Clark, H. C.; Ward, J. E. H.; Yasufuku, K. *Can. J. Chem.* **1975**, *53*, 186–191.
(26) Clark, H. C.; Ward, J. E. H. *J. Am. Chem. Soc.* **1974**, *96*, 1741–1748.
(27) Eaborn, C.; Odell, K. J.; Pidcock, A. *J. Chem. Soc., Dalton Trans.* **1978**, 357–368.

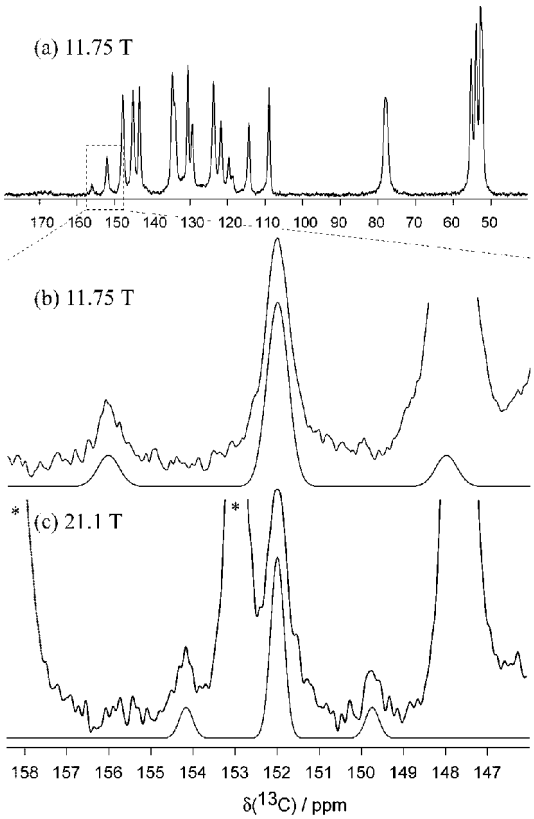

Figure 3. Solid-state ^{13}C RAMP-CP/MAS NMR spectra of **7**. (a) Full spectrum obtained at $B_0 = 11.75$ T with a MAS rate of 14 400 Hz. (b) Detailed expansion of the C_{ipso} region of the spectrum shown in (a); J coupling to ^{195}Pt is highlighted in the simulated spectrum shown below the experimental spectrum. (c) Same as (b), but acquired at $B_0 = 21.1$ T; MAS rate = 10 000 Hz. Spinning sidebands are denoted by asterisks.

a *cis*-bis(2-phenylpyridine)Pt^{II} complex.[28] In this complex the aryl ring is connected to the metal via a Pt–C bond, coplanar with the platinum coordination plane, similar to NCN-pincer platinum complexes. The value presently obtained for the pincer compound **7** is therefore relatively large for ^{195}Pt coupling to an aromatic carbon. Those for CO ligands are larger[29] (e.g., 1817 Hz for *trans*-[Pt(NCS)(CO)(PPh_3)$_2$][BF_4]) and those for carbenes may be either smaller (e.g., 666–759 Hz)[22,27] or larger (e.g., 1047–1125 Hz).[30] The value of 1003 Hz suggests that apart from the dominating M–C σ-interaction, this bond also receives a contribution from aryl−platinum π-interaction.[21] This view is supported by the previous UV/vis study on the stilbenoid pincer platinum complexes **2**–**8**.[6] This study reveals that the interaction of the metal center (as a donor group) with the conjugated backbone results in an intense low-energy charge transfer excitation.[5]

UV/Vis Properties. The absorption maxima (λ_{max}) and absorption coefficients (ϵ) of **1** (R′ = NPh_2) and **11** (R′ = CN) were measured, with the UV/vis spectra for **1** in various solvents and for **11** in CH_2Cl_2 (for data see Table 3). Their absorption spectra in dichloromethane are depicted in Figure 4, as well as the spectrum of **7** for comparison.

Table 3. UV/Vis Data of 1 in Various Solvents and 11 in CH_2Cl_2[a]

solvent	CH_3CN	CH_2Cl_2	THF	EtOAc	Et_2O	C_6H_{12}
		[PtCl(NCN($C_2H_2C_6H_4$-NPh_2-4′)-4)] (**1**)				
λ_{max} (nm)	374	397 [41.4][b]	393[b]	377	376	394[b]
	299	379 [51.7], 309 [21.1]	379	299	298	379
			307			305
		[$PtCl_3$(NCN($C_2H_2C_6H_4$-CN-4′)-4)] (**11**)				
λ_{max} (nm)		386 [3.0][b]				
		334 [42.1]				

[a] Absorption wavelength (nm) at room temperature ($c \approx 10^{-5}$ M), absorption coefficient ϵ between brackets (ϵ in 10^3 M^{-1} cm^{-1}). [b] Shoulder.

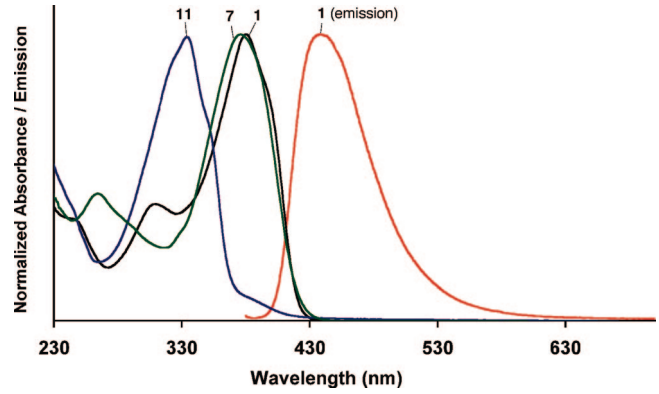

Figure 4. Normalized UV/vis absorption spectra of **1**, **7** (λ_{max} [$\epsilon \times 10^3$ M^{-1} cm^{-1}] = 376 nm [29.4], 264 nm [13.1]) from ref 5, and **11** in CH_2Cl_2; normalized emission spectrum of **1** in CH_2Cl_2.

It must be noted that **1** and **11** are soluble in dichloromethane, but their solubility decreases in less polar solvents like diethyl ether, whereas they are hardly soluble in cyclohexane. As a result of the limited solubility, reliable values of ϵ for **1** and **11** could only be determined in dichloromethane.

The absorption spectra of **1** (R′ = NPh_2) in various solvents (Table 3, Figure 4) show a weak band between 298 and 309 nm. By analogy with 4-(diphenylamino)stilbene, this is likely to be a transition localized in the triphenylamine part.[31] An intense lower energy band ($S_0 \rightarrow S_1$) is observed around 374–379 nm, in some solvents accompanied by a shoulder at 394–397 nm. Furthermore, the absorption measurements of **1** in different solvents showed no distinct solvent polarity dependence (Table 3), pointing to a weakly polar ground state of the molecule.

The solution of **11** (R′ = CN, M = Pt(IV)) in dichloromethane shows a strong transition band at 334 nm with a weak shoulder around 386 nm.

The UV/vis spectrum of **1** looks similar to that of 4-(diphenylamino)stilbene (λ_{max} = 362 nm, MeCN),[31] but is slightly shifted toward lower energy, which is the result of the presence of the platinum center.

Comparison of the UV/vis spectra of **1**, which contains the NPh_2 and NCN-PtCl fragment as donor groups, with the spectrum of compound **7**, which contains the electron-accepting CN group and the metal-pincer fragment as the donor, shows that the λ_{max} of **1** is situated at a longer wavelength than the λ_{max} of **7**. Normally it is expected that when a strong donor–acceptor (push–pull) interaction is present in a molecule (like in **7**), the HOMO–LUMO gap decreases, reflected by an intramolecular charge transfer (ICT) band at lower energy. In contrast to this, the λ_{max} of **1**, which contains two donor groups, is found

(28) Chassot, L.; Müller, E.; von Zelewsky, A. *Inorg. Chem.* **1984**, *23*, 4249–4253.
(29) Cherwinski, W. J.; Johnson, B. F. G.; Lewis, J.; Norton, J. R. *J. Chem. Soc., Dalton Trans.* **1975**, 1156–1158.
(30) Chisholm, M. H.; Clark, H. C.; Ward, J. E. H.; Yasufuku, K. *Inorg. Chem.* **1975**, *14*, 893–899.
(31) Yang, J. S.; Chiou, S. Y.; Liau, K. L. *J. Am. Chem. Soc.* **2002**, *124*, 2518–2527.

Table 4. Fluorescence Data of [PtCl(NCN($C_2H_2C_6H_4$-NPh_2-4′)-4)] (1)

solvent	λ_{fl} (nm)[a]	Φ_{fl}	τ_{fl} (ns)[b]	k_r (10^8 s^{-1})	k_{nr} (10^8 s^{-1})
acetonitrile	457	0.202	0.69	2.91	11.5
dichloromethane	437	0.026	2.00	0.13	4.9
tetrahydrofuran	440	0.010	1.50	0.07	6.6
ethyl acetate	472	0.010	1.66	0.06	6.0
diethyl ether	444	0.007	1.46	0.05	6.8
cyclohexane	438	0.008	[c]		

[a] Excitation wavelength 370 nm, argon-flushed solutions at room temperature, $c \approx 10^{-6}$ M. [b] Only the values for the slow component of the biexponential decay curve is reported, as the fast component was not significantly different from the instrument temporal response (<50 ps). [c] Solubility too low to allow for measurements.

Table 5. TD-DFT Excitation Energies (E) and Nonvanishing Oscillator Strength (f > 0.1) Calculated for 2, 5, and 7

compound	state	composition[a]	E [eV]	λ [nm]	f
2 (R′ = NMe_2)	2A	94% (H→L)	3.26	380	1.373
5 (R′ = H)	2A	94% (H→L)	3.32	374	0.868
	7A	77% (H−2→L)	4.10	302	0.382
7 (R′ = CN)	2A	96% (H→L)	2.93	423	0.855
	5A	90% (H−3→L)	3.75	331	0.516
	13A	48% (H→L+3)	4.31	288	0.142
		20% (H−6→L)			
		13% (H→L+2)			

[a] c^2 > 0.1; H = HOMO, L = LUMO.

at lower energy than **7**. Recently a similar behavior was observed by Yin and co-workers for cyclometalated Pt(II) complexes containing substituted 4-R-styryl-2-phenylpyridine ligands (R = NO_2, H, OMe, NEt_2), with the substituents also located on the *para* position of the metal center.[32]

In order to elucidate more of the UV/vis properties of the stilbenoid pincer platinum complexes, a theoretical study was performed on a selected series of stilbenoid pincer platinum compounds using TD-DFT calculations (vide infra).

Comparing the UV/vis spectra of **11** (R′ = CN, M = Pt(IV)) and **7** (R′ = CN, M = Pt(II)), it can be seen that a change of oxidation state of the platinum center largely influences the absorption spectrum of the complex (Figure 4). The CT band in **7** appears for **11** at a higher energy, which points to a loss of the charge transfer interaction between the metal center and the R′ substituent. Notable is that in the NMR and IR spectra of these compounds, the change of the oxidation state hardly affects the electronics of the R′-containing phenyl ring. The higher oxidation state of the platinum center of **11** makes it a weaker donor. The intense band of **11** at 334 nm can then be assigned to a $\pi-\pi^*$ transition of the donor decoupled 4-cyanostilbene fragment. Indeed for 4-cyanostilbene an intense absorption in the same region (λ_{max} = 323 nm, MeCN) has been reported.[33]

Fluorescence Properties. As **1** showed (but not **11**) luminescence at room temperature, only **1** was further studied for its photophysical properties by determination of the fluorescence maxima (λ_{fl}), quantum yields (Φ_{fl}), and excited-state lifetime (τ_{fl}) in solvents of different polarity. From this data the radiative (k_r) and nonradiative (k_{nr}) decay constants could be calculated (Table 4). The emission spectra of **1** contained a broad emission band in the region 437–472 nm (Figure 3). Although it was observed that these bands change position in a different solvent, no clear trend between the emission wavelength and the solvent polarity could be established.

Table 6. Calculated HOMO–LUMO Energy Data for the Platinum Complexes (2, 3, 5−8, and DANS)

compound	E_{HOMO} (eV)	E_{LUMO} (eV)	ΔE (eV)	λ (nm)	E_{exp}[a] (eV)	λ_{exp}[a] (nm)
2 (R′ = NMe_2)	−4.58	−1.10	3.48	356	3.34	371
3 (R′ = OMe)	−4.93	−1.37	3.56	348	3.52	352
5 (R′ = H)	−5.06	−1.50	3.56	348	3.54	350
6 (R′ = I)	−5.17	−1.72	3.45	359	3.46	358
7 (R′ = CN)	−5.36	−2.21	3.15	394	3.30	376
8 (R′ = NO_2)	−5.49	−3.08	2.41	514	3.00	413
DANS	−5.34	−2.87	2.47	502	2.84	437

[a] Experimental values in CH_2Cl_2 from ref 5.

The quantum yield and lifetimes of **1** in acetonitrile are different from the rest, suggesting a special interaction of this solvent with **1**. Except for complex **1** in acetonitrile, the quantum yields (0.007–0.026) are in the range expected for stilbenoid pincer platinum complexes.[6] However, the values are lower than those of 4-(diphenylamino)stilbene (Φ_{fl} = 0.53, MeCN),[31] suggesting that the presence of the platinum center favors nonradiative decay to the ground state.

The lifetimes for **1** (1.5–2.0 ns, Table 4) point to fluorescence and are, together with the derived values for the radiative and nonradiative decay rates, in agreement with the values found for the related organic 4-(diphenylamino)stilbene.[31,34] An increase of solvent polarity moderately influences the quantum yield and the fluorescence lifetime of **1**.

In general the stilbene compounds show a complex excited-state relaxation behavior,[35] as was explained before for stilbenoid pincer platinum complexes.[6] In the case of **1** the relaxation to the ground state via *cis*−*trans* isomerization becomes less important, reflected by the radiative and nonradiative decay rate constants (Table 4), similar to that found for 4-(diphenylamino)stilbene.[31]

Theoretical Calculations. A theoretical study was performed for a selected series of stilbenoid pincer platinum complexes, in order to better understand the solution UV/vis absorption spectra, which are determined by the electronic interactions between the *para* substituents and the metal center. To elucidate the nature of the first excited state, the UV/vis spectra of **2**(R′ = NMe_2), **5** (R′ = H), and **7** (R′ = CN) were calculated using TD-DFT (see Experimental Part). The calculated excitation energies and oscillator strengths, as well as their assignments, are given in Table 5. For the three compounds the most intense absorption band is the low-energy HOMO → LUMO transition. For **5** and **7** also transitions at higher energy are present, with a decreased oscillator strength, originating from transitions from lower lying occupied MOs to the LUMO, or from the HOMO to higher unoccupied MOs.

The relative positions of the low-energy transitions agree with the experimental solution data of these compounds (vide infra, Table 6).[6] The transition energy of the main band decreases in the order **5** (highest energy), followed by **2**, then **7** (lowest energy). The results show that going throughout the series the lowest energy transition is essentially a HOMO → LUMO transition.

In order to get insight into the charge transfer upon excitation, for push–pull compound **7** a plot of the electron density difference between the ground state and the excited state was

(32) Yin, B.; Niemeyer, F.; Williams, J. A. G.; Jiang, J.; Boucekkine, A.; Toupet, L.; Le Bozec, H.; Guerchais, V. *Inorg. Chem.* **2006**, *45*, 8584–8596.

(33) Hara, M.; Samori, S.; Cai, X. C.; Fujitsuka, M.; Majima, T. *J. Org. Chem.* **2005**, *70*, 4370–4374.

(34) Rumi, M.; Ehrlich, J. E.; Heikal, A. A.; Perry, J. W.; Barlow, S.; Hu, Z. Y.; McCord-Maughon, D.; Parker, T. C.; Röckel, H.; Thayumanavan, S.; Marder, S. R.; Beljonne, D.; Brédas, J. L. *J. Am. Chem. Soc.* **2000**, *122*, 9500–9510.

(35) Rettig, W.; Majenz, W.; Herter, R.; Létard, J. F.; Lapouyade, R. *Pure Appl. Chem.* **1993**, *65*, 1699–1704.

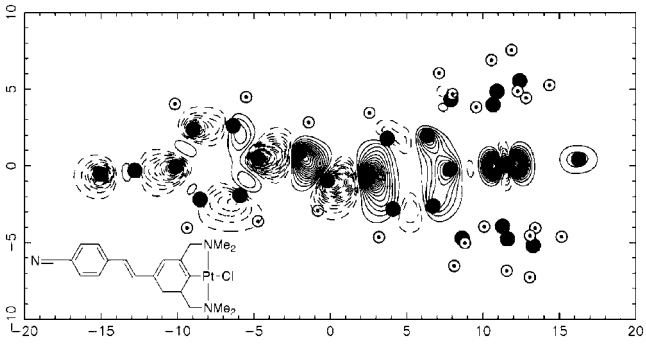

Figure 5. Electron density difference plot of **7**; ρ(ground state) − ρ(excited state); solid lines → loss of electrons upon excitation; dashed lines → gain of electrons upon excitation.

generated (Figure 5, for details see Supporting Information). In this plot it is shown that, upon excitation, the electron density decreases on the donating pincer platinum fragment and increases on the accepting nitrile fragment, reflecting the moving of charge from the donor to the acceptor side. This shows that the Pt moiety functions as a donor. The plot also shows that electron density shifts from one carbon to the other carbon atom of the ethylene bridge.

The same conclusion regarding the charge transfer character of the HOMO–LUMO transition of **7** can be drawn from the inspection of the orbitals involved in this transition. The HOMO of **7** (Figure 6) is mainly located on the donor fragment, with a small contribution of the ethylene linker, whereas the LUMO of **7** is mainly located on the nitrile fragment. Upon excitation the electron density decreases where the HOMO is localized and increases where the LUMO is located, which was also observed in Figure 5. Since the TD-DFT results showed that for **2** and **5** this lowest energy transition is also mainly composed of the HOMO–LUMO excitation, it is suggested that the orbital pictures can be used to deduce the nature of the transitions in stilbenoid pincer platinum complexes. The plots of compound **8**, which contain the electron-accepting R′ = NO_2 group and the donating NCN-PtCl fragment, show that the HOMO is mainly located at the donor side. The LUMO is mainly located at the acceptor side, suggesting charge transfer from the donor to the acceptor side upon excitation, i.e., intramolecular charge transfer (ICT). Noteworthy is the similarity between **8** and *trans*-4-dimethylamino-4′-nitrostilbene (DANS), which was used as an organic stilbenoid reference compound.[6,36]

The HOMOs of **6** (R′ = I), **5** (R′ = H), and **3** (R′ = OMe) are mainly located at the platinum side, similar to what was found for **7**, but in these compounds the HOMO has also very small tails on the R′ side. The LUMOs of **6**, **5**, and **3** are mainly located at the R′-substituted phenyl ring and are also slightly located on the NCN fragment (as was found previously for **7**). Upon excitation, for these compounds charge will mainly move from the platinum side toward the R′-substituted phenyl ring. For **2** (R′ = NMe_2), which contains two *para*-situated donor groups, the HOMO has contributions from both the metal center and the NMe_2 group. The LUMO of this compound is mainly located on the central ethylene linker (Figure 6). Therefore, for **2**, upon excitation, charge transfer from both donor groups to the central double bond is expected.

The effect of the different substituents R′ on the HOMO or LUMO of this class of compounds can be rationalized in terms of qualitative π molecular orbital correlation diagrams (Figure 7).[36,37] The π-energy levels of the unperturbed stilbenoid pincer platinum moiety (R′ = H, **5**) are a good starting point. Electron donors (D) provide a doubly occupied molecular orbital, which is higher in energy than the HOMO of the unperturbed stilbenoid pincer platinum fragment.[36] As these two orbitals interact, this results in a new higher lying HOMO. On the other hand, an electron acceptor (A) interacts, with its low-lying empty orbital, with the LUMO of the stilbenoid fragment, thereby stabilizing it, and since the HOMO level is only slightly affected, this also leads to a smaller HOMO–LUMO gap. Thus, a strong electron donor or acceptor yields a small HOMO–LUMO gap.

Because for **2**, **5**, and **7** the HOMO–LUMO excitation is found to be dominant in the first excited state (Table 5) and the transition energies correlate with the HOMO–LUMO gap, it is expected that the excitation energies of the other stilbenoid pincer platinum compounds also correlate with the HOMO–LUMO gap throughout the series (Table 6). Indeed for the other compounds it is seen that the trend in the experimental λ_{max}[5] follows that of the calculated HOMO–LUMO gap (Table 6).

A similar relation between the electronic character of the substituents and the excited-state energy of the metal complex was also observed by others from a study on cyclometalated Pt(II) complexes.[32,38] The metal complexes contained substituted 4-(*R*-styryl)-2-phenylpyridine ligands (R = NO_2, H, OMe, NEt_2). In these complexes the low-energy absorption band of the 4-NEt_2-styryl-2-phenylpyridine platinum complex was assigned to consist of a mixture of ILCT (Et_2N → CH═CH*) and MLCT (dπ(Pt) → π*) transitions.

Electrochemical Measurements. The cyclic voltammograms of solutions of **1**−**8** in dichloromethane were measured, and the obtained redox data are presented in Table 7. As a representative example the cyclic voltammogram of **1** is shown in Figure 8. To avoid exchange of different anions on the Pt center, which would influence the redox process,[39,40] tetrabutylammonium chloride (TBACl) was used as the supporting electrolyte. Under the applied conditions however, the use of TBACl in CH_2Cl_2 limits the potential window to +1.0 V, because at higher potentials the chloride atoms are electrochemically oxidized. The compounds were first oxidized, and all cyclic voltammograms showed a single irreversible oxidation peak in the anodic region, corresponding to the oxidation of the Pt(II) to the Pt(IV) species, and exchange of chloride anions. A similar irreversible two-electron oxidation is observed for related NCN-pincer platinum halide complexes.[41–43]

As a consequence of the high stability of the formed Pt(IV)Cl_3 species, the reduction of the species in the reverse process is not observed within the applied potential window.

For compound **2** two irreversible oxidation peaks are observed around 0.04, and 0.20 V, i.e., the first from the oxidation of the Pt(II) center, and the second probably results from the oxidation of the R′ = NMe_2 group.

(36) van Walree, C. A.; Franssen, O.; Marsman, A. W.; Flipse, M. C.; Jenneskens, L. W. *J. Chem. Soc., Perkin Trans. 2* **1997**, 799–807.

(37) Meier, H. *Angew. Chem., Int. Ed. Engl.* **1992**, *31*, 1399–1420.

(38) Lepeltier, M.; Le Bozec, H.; Guerchais, V.; Lee, T. K. M.; Lo, K. K. W. *Organometallics* **2005**, *24*, 6069–6072.

(39) Albrecht, M.; Rodríguez, G.; Schoenmaker, J.; van Koten, G. *Org. Lett.* **2000**, *2*, 3461–3464.

(40) Jude, H.; Bauer, J. A. K.; Connick, W. B. *Inorg. Chem.* **2002**, *41*, 2275–2281.

(41) Back, S.; Gossage, R. A.; Lutz, M.; del Rio, I.; Spek, A. L.; Lang, H.; van Koten, G. *Organometallics* **2000**, *19*, 3296–304.

(42) Back, S.; Lutz, M.; Spek, A. L.; Lang, H.; van Koten, G. *J. Organomet. Chem.* **2001**, *620*, 227–234.

(43) Jude, H.; Bauer, J. A. K.; Connick, W. B. *Inorg. Chem.* **2004**, *43*, 725–733.

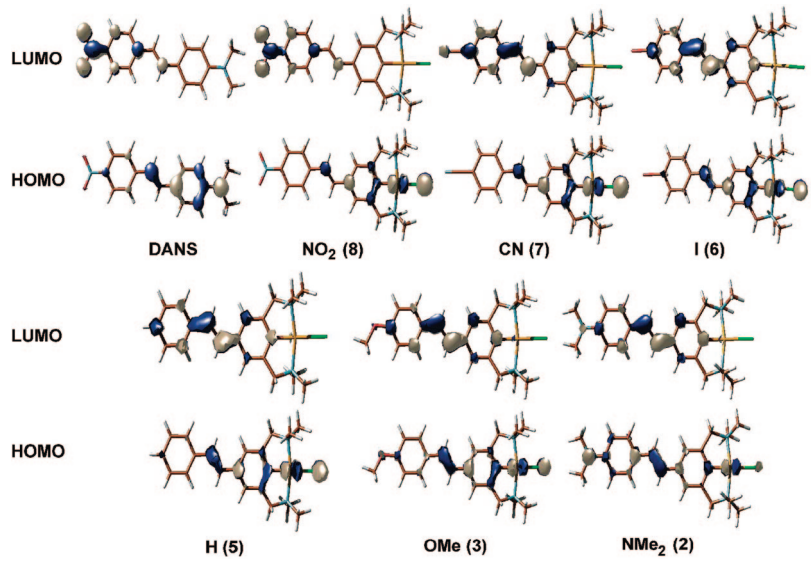

Figure 6. Contour plots of the HOMOs and LUMOs of **2**, **3**, **5**−**8**, and DANS.

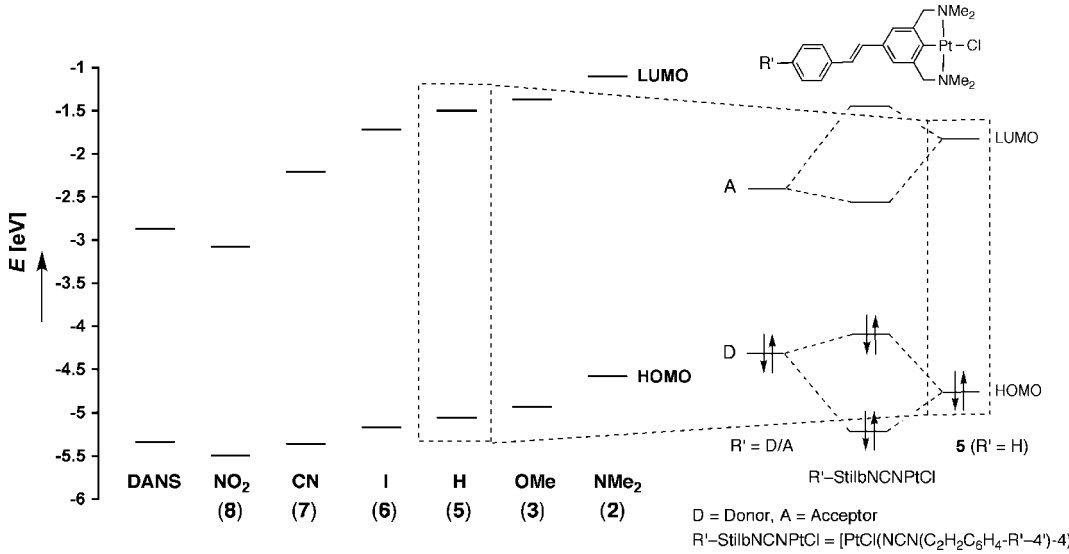

Figure 7. Correlation diagram for the highest occupied π-orbitals and lowest unoccupied π*-orbitals, including the calculated HOMO and LUMO energies of **2**, **3**, **5**−**8**, and DANS.

Table 7. Electrochemical Data for 1−8 in CH_2Cl_2[a]

	1 (R′ = NPh_2)	**2** (R′ = NMe_2)	**3** (R′ = OMe)	**4** (R′ = $SiMe_3$)	**5** (R′ = H)	**6** (R′ = I)	**7** (R′ = CN)	**8**[b] (R′ = NO_2)
E_{pa} (V)	0.13	0.04, 0.20	0.12	0.19	0.29	0.13	0.28	0.31
E_{pc} (V)	−0.92	−0.94	−0.84	−0.84	−1.05	−0.79	−0.86	−0.87

[a] Cyclic voltammograms have been recorded at rt, under argon, with nBu$_4$NCl as the supporting electrolyte (0.1 M); scan rate 100 mV s^{-1}. Potentials are reported in V vs Fc/Fc$^+$ (Fc = (η^5-C_5H_5)$_2$Fe, $E_{1/2}$= 0.00 V). E_{ox} and E_{red} are the peak potentials of the oxidation and reduction waves, respectively; [b] Reversible oxidation/reduction process for the NO_2 group ($E_{1/2}$ = −1.61 V, ΔE = 60 mV).

In general for **1**–**8** the oxidation potentials follow the expected trend, i.e., the complexes containing an electron-donating R′ group are oxidized at a lower potential (**1**−**4**), while molecules containing an electron-withdrawing R′ group (**7** and **8**) oxidize at a higher potential. Compounds **5** (R′ = H) and **6** (R′ = I) do not fit into this trend. Probably for **6** this is due to the electronic character of the iodine group.

For all the complexes an irreversible reduction is found in the cathodic region (−1.05 to −0.87 V, Figure 8), resulting from a reduction process we were not able to assign. It must be noted that these CV-derived potentials show no clear correlation with the calculated LUMO energies (Table 6). For **8**, which contains the NO_2 group, a reversible redox process was observed around −1.61 V (ΔE = 60 mV).

NLO Properties. Stilbenoid pincer platinum complexes **1**−**8** are expected to have interesting NLO properties because of the combination of the stilbenoid backbone and the Pt group. The presence of the different R′ groups makes it possible to perform a systematic study on the NLO properties of these molecules.

In the past it has already been shown that *para*-substituted stilbenoid and stilbazole ferrocene complexes show interesting NLO properties, resulting from a polar interaction of the metal fragment and the *para* substituent.[44] In these complexes the metal center is situated out of plane of the conjugated backbone

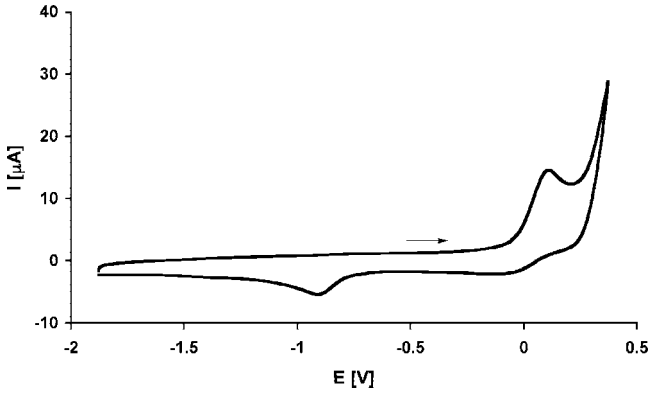

Figure 8. Cyclic voltammogram of **1** recorded in CH_2Cl_2 at room temperature (0.1 M TBACl; scan rate = 100 mV s^{-1}).

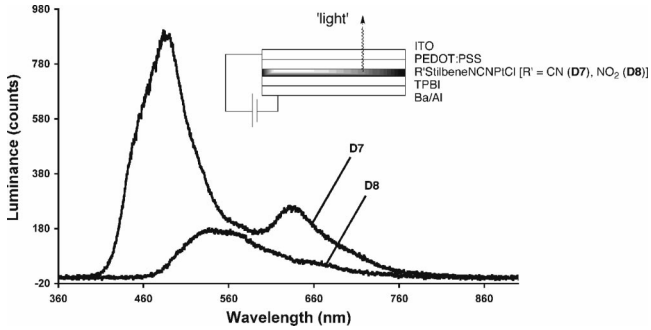

Figure 9. Electroluminescence spectra of **D7** and **D8**. Inset: schematic cross section of the fabricated OLEDs **D7** and **D8**, containing **7** (R′ = CN) and **8** (R′ = NO_2) as the emissive layers, respectively.

and the *para* substituent; only a few examples are known with the metal incorporated into the plane of the π-system.[45] In this arrangement the metal center does not lie on the molecular axis along which the dominant component of the hyperpolarizability is situated, i.e., the conjugated backbone of the molecule.[46] In this respect the pincer metal system offers a potential interesting feature, i.e., the pincer ligand keeps the metal center in the same plane with the *para*-situated R′ group, connected to each other via the conjugated backbone.

The β_{zzz} component of the hyperpolarizability tensor (where z is the direction of the charge transfer of **1**−**8**) was determined with the femtosecond hyper-Rayleigh scattering (HRS) technique, using an 800 nm Ti^{3+}:sapphire laser.[47,48] Accurate β_{zzz} values could be determined by measuring the individual samples in dichloromethane, at five different concentrations and different modulation frequencies, in order to exclude contributions of multiphoton fluorescence from the nonlinear scattering signal.[49,50]

Table 8. HRS and UV/Vis Data of 1−8 in CH_2Cl_2[a]

compound	β_{zzz} (10^{-30} esu)	β_0 (10^{-30} esu)	λ_{max} (nm)[b]	ϵ (10^3 M^{-1} cm^{-1})[b]
1 (R′ = NPh_2)	1106 (124)	88 (10)	379	51.7
2 (R′ = NMe_2)	667 (12)	73 (2)	371	36.9
3 (R′ = OMe)	164 (14)	80 (3)	352	30.6
4 (R′ = $SiMe_3$)	270 (20)	46 (3)	355	36.0
5 (R′ = H)	272 (14)	52 (3)	350	35.6
6 (R′ = I)	1324 (7)	211 (1)	358	37.3
7 (R′ = CN)	940 (60)	85 (5)	376	29.4
8 (R′ = NO_2)	[c]		413	20.6
DANS		56[d]	437[d]	27.1[d]
		21[e]	496[f]	

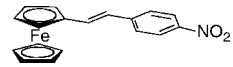

[a] DANS and [Fe(C_5H_5)(C_5H_4-C_2H_2-*p*-$C_6H_4NO_2$)] were included for comparison; HRS values of **1**−**7** determined at laser frequency = 800 nm. [b] Values of **2**−**8** in CH_2Cl_2 from ref 5. [c] No reliable HRS signal could be determined, resulting from too strong absorption of the compound at 400 nm. [d] Value from ref 36. in $CHCl_3$. [e] Calculated from $\beta_{1.91\mu m} = 31 \times 10^{-30}$ esu (ref 46) using eq 4. [f] from ref 3 in MeCN.

The obtained β_{zzz} values are listed in Table 8. Unfortunately for **8** no reliable HRS signal could be determined, due to too strong absorption of the compound at 400 nm (doubled laser frequency).

The stilbenoid pincer platinum complexes show a good hyperpolarizability, reflected by the β_{zzz} values of **1**−**7** ranging from 164 to 1324 (10^{-30} esu). Calculation of the static quadratic hyperpolarizability, β_o, gives values ranging from 46 to 211 (10^{-30} esu), which are of the same order of magnitude or higher than those of organic 4,4′-disubstituted stilbenes, like *trans*-4-dimethylamino-4′-nitrostilbene (DANS, included in Table 8),[51] and other organic NLO compounds.[52] These enhanced NLO properties can be the result of the polarization along the C−Pt bond of the NCN-PtCl moiety.[53,54]

The β values are also in line with and sometimes higher than other organometallic molecules[52] including the stilbenoid and stilbazole ferrocene analogues.[2,46,55] An example of a *p*-NO_2-substituted stilbenoid ferrocene analogue, [Fe(C_5H_5)(C_5H_4−C_2H_2-*p*-$C_6H_4NO_2$)],[3] is included in Table 8. The larger hyperpolarizability values of the stilbenoid pincer platinum complexes compared to those of [Fe(C_5H_5)(C_5H_4-C_2H_2-*p*-$C_6H_4NO_2$)] can be the result from the in-plane alignment of the PtCl fragment with the *para*-situated R′ substituent. A number of ruthenium−organic compounds has been reported that show β_o values in excess of 400 and even 500 (10^{-30} esu).[56] In addition, NLO properties

(44) Kanis, D. R.; Lacroix, P. G.; Ratner, M. A.; Marks, T. J. *J. Am. Chem. Soc.* **1994**, *116*, 10089–10102.

(45) (a) Whittall, I. R.; Humphrey, M. G.; Persoons, A.; Houbrechts, S. *Organometallics* 1996, *15*, 1935–1941. (b) Whittall, I. R.; Humphrey, M. G.; Houbrechts, S.; Persoons, A.; Hockless, D. C. R. *Organometallics* **1996**, *15*, 5738–5745. (c) Whittall, I. R.; Cifuentes, M. P.; Humphrey, M. G.; Luther-Davies, B.; Samoc, M.; Houbrechts, S.; Persoons, A.; Heath, G. A.; Bogsanyi, D. *Organometallics* **1997**, *16*, 2631–2637. (d) Garcia, M. H.; Robalo, M. P.; Dias, A. R.; Duarte, M. T.; Wenseleers, W.; Aerts, G.; Goovaerts, E.; Cifuentes, M. P.; Hurst, S.; Humphrey, M. G.; Samoc, M.; Luther-Davies, B. *Organometallics* **2002**, *21*, 2107–2118.

(46) Kanis, D. R.; Ratner, M. A.; Marks, T. J. *J. Am. Chem. Soc.* **1992**, *114*, 10338–10357.

(47) Clays, K.; Persoons, A. *Phys. Rev. Lett.* **1991**, *66*, 2980–2983.

(48) Hendrickx, E.; Clays, K.; Persoons, A. *Acc. Chem. Res.* **1998**, *31*, 675–683.

(49) Flipse, M. C.; de Jonge, R.; Woudenberg, R. H.; Marsman, A. W.; van Walree, C. A.; Jenneskens, L. W. *Chem. Phys. Lett.* **1995**, *245*, 297–303.

(50) Noordman, O. F. J.; van Hulst, N. F. *Chem. Phys. Lett.* **1996**, *253*, 145–150.

(51) Cheng, L. T.; Tam, W.; Stevenson, S. H.; Meredith, G. R.; Rikken, G.; Marder, S. R. *J. Phys. Chem.* **1991**, *95*, 10631–10643.

(52) Verbiest, T.; Houbrechts, S.; Kauranen, M.; Clays, K.; Persoons, A. *J. Mater. Chem.* **1997**, *7*, 2175–2189.

(53) Tromp, M.; Slagt, M. Q.; Klein Gebbink, R. J. M.; van Koten, G.; Ramaker, D. E.; Koningsberger, D. C. *Phys. Chem. Chem. Phys.* **2004**, *6*, 4397–4406.

(54) Tromp, M.; van Bokhoven, J. A.; Slagt, M. Q.; Klein Gebbink, R. J. M.; van Koten, G.; Ramaker, D. E.; Koningsberger, D. C. *J. Am. Chem. Soc.* **2004**, *126*, 4090–4091.

(55) Farrell, T.; Manning, A. R.; Murphy, T. C.; Meyer-Friedrichsen, T.; Heck, J.; Asselberghs, I.; Persoons, A. *Eur. J. Inorg. Chem.* **2001**, 2365–2375.

(56) (a) McDonagh, A. M.; Cifuentes, M. P.; Humphrey, M. G.; Houbrechts, S.; Maes, J.; Persoons, A.; Samoc, M.; Luther-Davies, B. *J. Organomet. Chem.* **2000**, *610*, 71–79. (b) Coe, B. J.; Jones, L. A.; Harris, J. A.; Brunschwig, B. S.; Asselberghs, I.; Clays, K.; Persoons, A.; Garín, J.; Orduna, J. *J. Am. Chem. Soc.* **2004**, *126*, 3880–3891.

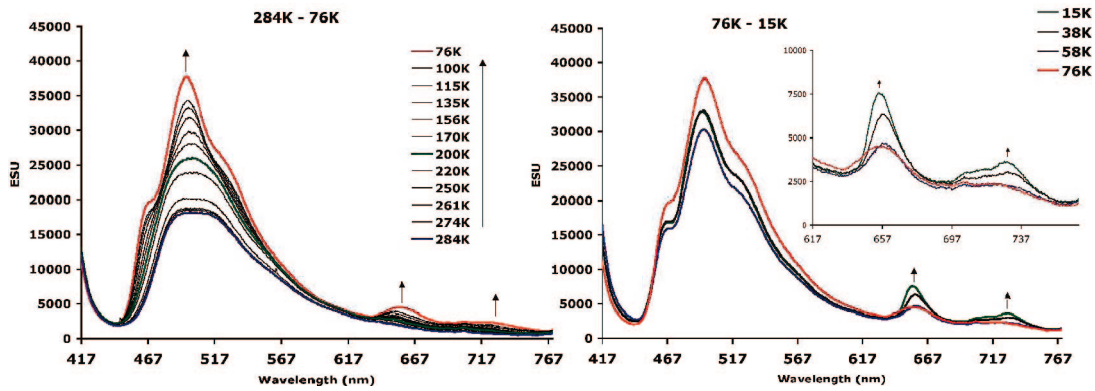

Figure 10. Solid-state emission of **7** at different temperatures (284–15 K).

Table 9. Electroluminescence Properties and Performances of Device D7 and D8

		device performance			
device	λ_{EL}[a] [nm]	voltage [V]	current intensity [mA cm^{-2}]	luminescence [cd m^{-2}]	EQE[b] [%]
D7	492, 643	10	6.3	4	0.030
D8	550	20	5.2	0.44	0.016

[a] λ_{max} electroluminescence. [b] External quantum efficiency.

of a few square-planar platinum(II) species have also appeared in the literature.[57]

Going from **1** to **7**, the β_{zzz} value changes from high, to low, to higher values again, with the largest values reported for **1** (R′ = NPh_2; $\beta_{zzz} = 1106 \times 10^{-30}$ esu) and **6** (R′ = I; $\beta_{zzz} = 1324 \times 10^{-30}$ esu). At first sight no clear relationship is present between the electronic properties of the R′ substituent and the obtained β values. For **1** the high β value can be correlated with the large absorption coefficient (ϵ), because ϵ is directly related with the oscillator strength *f*. This is in agreement with the two-level model,[55] which reflects that a low-energy CT transition, a large change of the molecular dipole moment upon excitation, or a large oscillator strength enhances the hyperpolarizability. For **6** the high β value, which is also contributed by the large ϵ value, probably also experiences a special contribution from the highly polarizable iodine atom, resulting in a large $\Delta\mu$.

It can be concluded that the contributions to the hyperpolarizability of the stilbenoid pincer platinum complexes cannot be completely explained by the two-state model, indicating that the contributions from other excited states also play a significant role.

Organic Light-Emitting Diode (OLED). The donor–acceptor stilbenoid pincers **7** (R′ = CN) and **8** (R′ = NO_2) showing emission in the visible region were applied in an optical device, i.e., an organic light -emitting diode (OLED; Figure 9). Layers of **7** and **8** were spin coated on the device as the emissive layer. In the forthcoming text we will refer to the devices containing **7** and **8** as **D7** and **D8**, respectively. The device fabrication is further described in the Supporting Information. The devices were studied for their electro-optical properties, and the results are displayed in Table 9.

D7 shows a white/blue emission color, with an intense band in the electroluminescence spectrum at 492 nm and a less intense band at 643 nm (Figure 9). **D8** shows a light green emission, with a broad band in the electroluminescence spectrum at 550 nm and a shoulder at 660 nm (Figure 9). For both devices, the most intense band probably results from a singlet-state CT excitation, at similar wavelengths to those observed in the solution emission spectra of **7** (λ_{em} = 443–476 nm) and **8** (λ_{em} = 546–677 nm).[6] In the solution spectra of **7** the extra band at 643 nm was never observed. This band can be the result of excimer formation or from emission from a triplet excited state. In order to obtain more information on the appearance of this long-wavelength band, the optical solid-state properties of **7** were studied in more detail (vide infra). For the devices it was found that even at a high voltage the luminescence intensity is still quite low. Comparing the device performances of **D7** and **D8** with cyclometalated platinum(II) complexes bearing a 3,5-di(2-pyridyl)-4-tolyl ligand[58] and a 2,2′-bipyridyl-6-phenyl ligand[59] the performances of **D7** and **D8** are rather low. These should be optimized to become of interest for practical applications.

Solid-State Emission Measurements. To deduce more information on the solid-state emission properties of **7**, powder emission measurements were performed at temperatures ranging from 284 to 15 K (Figure 10). The room-temperature solid-state emission spectrum of **7** shows a broad nonstructured emission band at 490 nm, similar to what was found in OLED **D7** (Figure 9). Upon cooling from 284 to 76 K the emission intensity increases, with the main band around 490 nm, and the emission band becomes more structured as a result of the narrowing of individual vibronic lines. Furthermore two weak emission bands come up at 660 and 730 nm, which also increase in intensity upon cooling. When the temperature is lowered below 76 K, the emission band at 490 nm decreases in intensity, while the two additional bands at longer wavelengths become more intense as the temperature decreases. Since the bands at 660 and 730 nm are not observed at room temperature, both in the solid state and in the solution emission spectra, it is unlikely that these bands result from the formation of excimers, because these would show an emission band at room temperature as well. Probably the low-energy bands represent phosphorescence from a spin-forbidden triplet excited state, which becomes observable due to the reduced nonradiative decay rates at low

(57) (a) Nguyen, P.; Lesley, G.; Marder, T. B.; Ledoux, I.; Zyss, J. *Chem. Mater.* **1997**, *9*, 406–408. (b) Cummings, S. D.; Cheng, L.-T.; Eisenberg, R. *Chem. Mater.* **1997**, *9*, 440–450. (c) Base, K.; Tierney, M. T.; Fort, A.; Muller, J.; Grinstaff, M. W. *Inorg. Chem.* **1999**, *38*, 287–289. (d) Roberto, D.; Ugo, R.; Tessore, F.; Lucenti, E.; Quici, S.; Vezza, S.; Fantucci, P. C.; Invernizzi, I.; Bruni, S.; Ledoux-Rak, I.; Zyss, J. *Organometallics* **2002**, *21*, 161–170.

(58) Sotoyama, W.; Satoh, T.; Sawatari, N.; Inoue, H. *Appl. Phys. Lett.* **2005**, *86*, 153505/1–153505/3.

(59) Lu, W.; Mi, B. X.; Chan, M. C. W.; Hui, Z.; Zhu, N. Y.; Lee, S. T.; Che, C. M. *Chem. Comm.* **2002**, 206–207.

temperatures. A similar triplet excited state can also be observed, quite limited, however, in organic stilbenes.[37,60]

Conclusions

The series of *para*-substituted stilbenoid pincer platinum complexes was successfully expanded with a new *para*-diphenylamino-functionalized stilbenoid pincer platinum complex **1** ($R' = NPh_2$). The UV/vis spectra of **1** show an intense low-energy λ_{max}, and the complex showed fluorescent properties comparable with those of the other stilbenoid pincer platinum complexes.

For stilbenoid pincer platinum complex **7** ($R' = CN$) the magnitude of the $^1J(^{13}C_{ipso},^{195}Pt)$ coupling constant revealed that the C_{ipso}−Pt bond mainly comprises the carbon−metal σ-interaction, but also contains contributions from a carbon−metal π-interaction. The electronic, UV/vis, and geometrical properties of Pt(II)Cl complex **7** are significantly changed when the complex is chemically oxidized to $Pt(IV)Cl_3$ complex **11**. In contrast to **7** compound **11** has no fluorescent properties at room temperature.

From the TD-DFT calculations on the series of stilbenoid pincer platinum complexes it appeared that both electron-donating and -accepting R′ substituents reduce the HOMO–LUMO gap of these compounds. Therefore the λ_{max} of $R' = H$ is found at the shortest wavelength and the absorption maxima of the other complexes are found at longer wavelength with the λ_{max} of $R' = NMe_2$ and NO_2 at the lowest energy, similar to what is observed in the experimental UV/vis spectra.

The complexes are more easily electrochemically oxidized when the *para* substituent R′ changes from electron accepting ($R' = NO_2$) toward electron donating ($R' = NPh_2$).

The NLO properties do not show a specific correlation between the electron-donating or -accepting properties of R′ and the β_{zzz} values. The magnitude of β_{zzz} seems to depend on both the relative energy of the first excited-state transition and the magnitude of the absorption coefficients of the stilbenoid pincer complexes. The presence of the PtCl moiety in the stilbenoid pincer complexes enhances the NLO properties compared to other organic and organometallic compounds. It is expected that these enhancements are the result of polarization of the C_{ipso}−Pt bond.

In addition, two stilbenoid pincer platinum complexes were successfully applied in an organic light emitting diode (OLED). The devices, which actually gave light, have to improve on their performance in order to become interesting for practical applications.

By the introduction of the NCN-pincer platinum fragment into electronically tunable stilbenoid compounds it was shown that organometallic complexes can be obtained with interesting optical and promising NLO properties.

Experimental Section

General Procedures. All reactions involving air- or moisture-sensitive reagents were performed by standard Schlenk techniques unless stated otherwise. Light-sensitive compounds and solutions were protected from light by use of aluminum foil. Pentane and THF were distilled from Na/benzophenone, and CH_2Cl_2 was distilled from CaH_2 prior to use. The aldehyde pincer platinum complex [PtCl(NCN-CHO-4)] (**10**) and stilbenoid pincer platinum complex [PtCl(NCN($C_2H_2C_6H_4$-CN-4′)-4)] (**1**) and diethyl-4-diphenylaminobenzylphosphonate (**9**) were prepared according to published procedures.[6,14,15] All other reagents were commercially available and used without further purification. ^1H and $^{13}C\{^1H\}$ NMR spectra were recorded at 25 °C on Bruker AC 300 NMR, Varian Inova 300, or Varian 400 spectrometers (operating frequencies: for ^1H spectra at 400 and 300 MHz; for ^{13}C spectra at 101 and 75 MHz), and chemical shifts are reported in ppm and referenced to residual solvent resonances. $^{195}Pt\{^1H\}$ NMR spectra were recorded on a Varian Inova 300 MHz NMR spectrometer (operating at 64.4 MHz), referenced to external Na_2PtCl_6 (1 M in D_2O, $\delta = 0$ ppm).[61]

Elemental analyses were performed by Kolbe, Mikroanalytisches Laboratorium (Mülheim a.d. Ruhr, Germany). ES-MS spectra were obtained from the Biomolecular Mass Spectrometry Group at Utrecht University. Infrared spectra were recorded with a Perkin-Elmer Spectrum 1 FT-IR spectrometer. The CV measurements were performed with an Autolab PGstat10 potentiostat controlled by GPES4 software. A three-electrode system was used, consisting of a platinum working electrode, a platinum (Pt) auxiliary electrode, and an Ag/AgCl reference electrode. The experiments were carried out in dichloromethane at rt under argon with tetrabutylammonium chloride (TBACl) as the supporting electrolyte (0.1 M). All redox potentials are reported against the ferrocene/ferrocenium (Fc/Fc^+) redox couple used as an internal standard ($E_{1/2} = 0.00$ V). Linear voltammograms were obtained at a scan rate of 100 mV s^{-1}. UV spectra were collected on Cary 1 or Cary 5 spectrophotometers in spectrophotometric grade solvents. Fluorescence emission spectra were obtained on a Spex Fluorolog instrument, equipped with a Spex 1680 double excitation monochromator, a Spex 1681 emission monochromator, and a Spex 1911F detector. Fluorescence spectra were corrected for the detector spectral response with the aid of a correction file provided by the manufacturer. Fluorescence quantum yields were determined relative to 9,10-diphenylanthracene ($\Phi_{fl} = 0.90$, excitation wavelength 370 nm).[62] Solvents used for fluorescence measurements were of spectrophotometric grade (Acros).

[PtCl(NCN($C_2H_2C_6H_4$-NPh_2-4′)-4)] (1). To a mixture of metalloaldehyde **10** (100 mg, 0.22 mmol) and diethyl 4-(diphenylamino)benzylphosphonate **9** (97 mg, 0.25 mmol) in THF (15 mL) was added *t*-BuOK (62 mg, 0.56 mmol), directly causing a color change of the reaction mixture to orange. After stirring for 2 h the reaction mixture was quenched at 0 °C by the subsequent addition of ice and an aqueous NaCl solution. The formed precipitate was isolated by filtration and subsequently washed with H_2O and pentane. The residue was dissolved in CH_2Cl_2, dried using $MgSO_4$, filtered, and evaporated to dryness, leaving the crude product. The product was precipitated from CH_2Cl_2 by the addition of pentane, and **1** was isolated, after centrifugation, as a yellow powder (143 mg, 0.20 mmol, 93%). ^1H NMR (400 MHz, CD_2Cl_2): δ 7.39 (d, $^3J(H,H) = 8.4$ Hz, 2H; ArH), 7.28 (t, $^3J(H,H) = 7.6$ Hz, 4H; ArH), 7.10 (d, $^3J(H,H) = 7.6$ Hz, 4H; ArH), 7.07–7.01 (m, 5H; ArH, CH=), 7.00 (s, 2H; ArH), 6.92 (d, $^3J(H,H) = 16.0$ Hz, 1H; *trans* CH=), 4.05 (s, $^3J(H,Pt) = 42.3$ Hz, 4H; CH_2), 3.06 (s, $^3J(H,Pt) = 31.6$ Hz, 12H; CH_3). $^{13}C\{^1H\}$ NMR (101 MHz, CD_2Cl_2): δ 148.0, 147.3, 146.6 (C_{ipso} to Pt), 144.3, 133.4, 132.7, 129.6, 128.7, 127.2, 125.4, 124.7, 124.1, 123.3, 117.7, 77.9, 54.6. $^{195}Pt\{^1H\}$ NMR (64 MHz, CD_2Cl_2): δ –3163. IR (ATR): $\tilde{\nu}$ 3020, 2917, 1588, 1507, 1490, 1467, 1449, 1400, 1326, 1273, 1177, 1156, 1107, 1084, 1013, 959, 889, 837, 752, 694 cm^{-1}. MS (ES+; CH_2Cl_2) *m/z*: 689.34 $[M + H]^+$, 654.33 $[M + H - Cl]^+$. Anal. Calcd (%) for $C_{32}H_{34}ClN_3Pt$ (691.16): C 55.61, H 4.96, N 6.08. Found: C 55.48, H 5.06, N 6.00.

[$PtCl_3$(NCN($C_2H_2C_6H_4$-CN-4′)-4)] (11). To a solvent mixture (10 mL, MeOH/CH_2Cl_2, 1:1) containing **7** (63 mg, 0.11 mmol) was added $CuCl_2 \cdot 2H_2O$ (40 mg; 0.23 mmol), and the solution was stirred for 24 h. The solution was filtered to remove the precipitated CuCl and the filtrate was evaporated to dryness in vacuo. The

(60) Ramamurthy, V.; Caspar, J. V.; Corbin, D. R. *Tetrahedron Lett.* **1990**, *31*, 1097–1100.
(61) Pregosin, P. S. *Coord. Chem. Rev.* **1982**, *44*, 247–291.
(62) Eaton, D. F. *Pure Appl. Chem.* **1988**, *60*, 1107–1114.

residual solid was taken up in CH_2Cl_2 (15 mL) and washed with water (3 × 5 mL). The organic layer was dried with $MgSO_4$ and concentrated in vacuo, and the product was precipitated with pentane. After centrifugation **11** was isolated as an orange powder, 49 mg (0.079 mmol, 69%). ^{1}H NMR (300 MHz, CD_2Cl_2): δ 7.68 (d, ^3J(H,H) = 8.7 Hz, 2H; ArH), 7.62 (d, ^3J(H,H) = 8.7 Hz, 2H; ArH), 7.29 (d, ^3J(H,H) = 16.2 Hz, 1H; *trans* CH=CH), 7.27 (s, 2H; ArH), 7.09 (d, ^3J(H,H) = 16.2 Hz, 1H; *trans* CH=CH), 4.42 (s, ^3J(H,Pt) = 29.7 Hz, 4H; CH_2), 3.06 (s, ^3J(H,Pt) = 28.5 Hz, 12H; CH_3). ^{13}C{^{1}H} NMR (75 MHz, CD_2Cl_2): δ 144.9 (C_{ipso}), 141.8, 141.0 (^2J(C,Pt) = 16.3 Hz; C_{ortho}), 136.8, 132.9, 131.7, 127.5, 127.3, 121.2 (^3J(C,Pt) = 16.3 Hz; C_{meta}), 119.2 (CN), 111.9, 76.6 (^2J(C,Pt) = 19.6 Hz; NCH_2), 56.8 ($N(CH_3)_2$). ^{195}Pt{^{1}H} NMR (64 MHz, CD_2Cl_2): δ –1504. IR (ATR): $\tilde{\nu}$ = 3033, 3003, 2927, 2222 (CN), 1669, 1630, 1600, 1583, 1504, 1454, 1408, 1326, 1272, 1224, 1175, 1085, 1069, 965, 888, 863, 853, 831, 723, 705 cm^{-1}. MS (ES+; CH_2Cl_2) *m/z*: 584.13 [M − Cl]$^+$. Anal. Calcd (%) for $C_{21}H_{24}Cl_3N_3Pt$ (619.87): C 40.69, H 3.90, N 6.78. Found: C 39.25, H 4.18, N 6.57.

X-ray crystal structure determination of 11: $C_{21}H_{24}Cl_3N_3Pt$, fw = 619.87, red block, 0.21 × 0.21 × 0.12 mm^3, orthorhombic, $Pna2_1$ (no. 33), a = 25.7528(4), b = 6.94510(10), c = 24.4159(7) Å, V = 4366.92(15) Å^3, Z = 8, D_x = 1.886 g/cm^3, μ = 6.81 mm^{-1}. Reflections (69 248) were measured on a Nonius Kappa CCD diffractometer with rotating anode (graphite monochromator, λ = 0.71073 Å) up to a resolution of $(\sin \theta/\lambda)_{max}$ = 0.65 Å^{-1} at a temperature of 150 K. An absorption correction based on multiple measured reflections was applied (0.21–0.44 correction range); 9947 reflections were unique (R_{int} = 0.0391). The structure was solved with automated Patterson methods(program DIRDIF-99)[63] and refined with SHELXL-97[64] against F^2 of all reflections. Non-hydrogen atoms were refined with anisotropic displacement parameters. All hydrogen atoms were introduced in calculated positions and refined with a riding model. The crystal was refined as an inversion twin converging at a twin fraction of 0.389(5). The diffraction images contained diffuse streaks, which could not be taken into account, resulting in rather large residual electron densities close to the platinum centers; 514 parameters were refined with 1 restraint. R1/wR2 [$I > 2\sigma(I)$]: 0.0309/0.0625. R1/wR2 [all reflns]: 0.0404/0.0654. S = 1.109. Residual electron density between –0.56 and 2.28 e/Å^3. Geometry calculations and checking for higher symmetry was performed with the PLATON program.[65]

Acknowledgment. We thank Prof. Dr. J. Reedijk and Dr. S. Tanase from Leiden University for the assistance with electrochemical measurements. This work was partially supported (G.D.B., M.L., and A.L.S.) by the Council for Chemical Sciences of The Netherlands Organization for Scientific Research (NWO/CW). R.W.A.H. acknowledges financial support from The Netherlands Organization for Scientific Research (NWO), grant 700.53.401. We acknowledge NWO/NCF for supercomputer time on TERAS/ASTER, SARA (The Netherlands, project number SG-032). Access to the 900 MHz NMR spectrometer was provided by the National Ultrahigh Field NMR Facility for Solids (Ottawa, Canada), a national research facility funded by the Canada Foundation for Innovation, the Ontario Innovation Trust, Recherche Québec, the National Research Council Canada, and Bruker BioSpin and managed by the University of Ottawa (www.nmr900.ca). NSERC is acknowledged for a MRS grant and for funding to D.L.B.

Supporting Information Available: Information about the lifetime measurements, solid-state NMR spectroscopy of **7**, HRS measurements, device fabrication, theoretical calculations, and X-ray crystal structure determination of **11**. This material is available free of charge via the Internet at http:/pubs.acs.org.

OM700352Z

(63) Beurskens, P. T.; Admiraal, G.; Beurskens, G.; Bosman, W. P.; Garcia-Granda, S.; Gould, R. O.; Smits, J. M. M.; Smykalla, C., *The DIRDIF99 program system*, Technical Report of the Crystallography Laboratory; University of Nijmegen: The Netherlands, 1999.

(64) Sheldrick, G. M. *SHELXL-97. Program for crystal structure refinement*; University of Göttingen: Germany, 1997.

(65) Spek, A. L. *J. Appl. Crystallogr.* **2003**, *36*, 7–13.